Preprint Title	Determination of nonlinear absorption and scattering in a single plasmonic nanostructure using X-scan technique
Authors	Tushar C. Jagadale, Dhanya Murali and Shi-Wei Chu
Publication Date	30 Jul 2019
Article Type	Full Research Paper
ORCID® iDs	Shi-Wei Chu - https://orcid.org/0000-0001-7728-4329

Determination of nonlinear absorption and scattering in a single plasmonic nanostructure using X-scan technique

Tushar C Jagadale[1,2], Dhanya Murali[1], Shi-Wei Chu[1,3,*]

Address:

[1]Department of Physics, National Taiwan University, No.1, Sec. 4, Roosevelt Rd., Taipei 10617, Taiwan (R.O.C.),

[2]Technical Physics Division, Bhabha Atomic Research Centre, Mumbai 400085, India,

[3]Molecular Imaging Centre, National Taiwan University, No.1, Sec. 4, Roosevelt Rd., Taipei 10617, Taiwan (R.O.C.)

Email: Shi-Wei Chu * –swchu@phys.ntu.edu.tw

* Corresponding author

Abstract

Nonlinear nano-plasmonics opens up many exciting opportunities, such as nano-laser, nano-antenna, nano-modulator, etc. A highly desirable tool in the field of nonlinear nano-plasmonics is to characterize nonlinearity of optical absorption and scattering in single nanostructures. Currently, the most widely used method to quantify optical nonlinearity is z-scan, which can derive real and imaginary parts of permittivity through translating a thin sample across a laser focus. However, z-scan typically works with thin films, and thus acquires nonlinear responses from ensemble of nanostructures, not a single one. In this work, we present an X-scan technique,

which is based on laser scanning microscopy equipped with forward and backward detectors. The two-channel detection allows simultaneous quantification of nonlinear behaviours of scattering, absorption, as well as total attenuation, from a single nanostructure. At low excitation intensity, both scattering and absorption responses are linear, thus confirming the linearity of detection system. At high excitation intensity, we found that the nonlinear response can be derived directly from the point spread function of X-scan images. Surprisingly high level of nonlinearities in both scattering and absorption are unravelled simultaneously for the first time. Our study not only provides a novel method for characterizing single-nanostructure nonlinearity, but also reports exceptionally large plasmonic nonlinearities.

Keywords

single gold nanostructure; nonlinear absorption; absorption cross-section; nonlinear scattering; laser scanning microscopy.

Introduction

It is well known that optical properties of nano-metals, i.e. plasmonic nanostructures, differ significantly from its bulk counterpart, due to two main reasons, i.e. enhancement in the surface to volume ratio and appearance of quantum effects such as surface plasmon resonance (SPR). For example, color, or equivalently scattering/absorption spectra, of nano-sized metals can be very different from their bulk counterparts. Plasmonic nanostructures, in general, can offer strong scattering, great photo-stability, high brightness, exceptional localisation precision and long observation time. In addition, SPR boosts uplocal electric field, and thus optical nonlinear interactions are significantly enhanced with metallic nanostructures [1-3].

An emerging field of nonlinear nanoplasmonics deals with the nanoscale confined optical field enhancement as well as the giant nonlinearity provided by plasmonic nanostructures [4-6].

The potential applications of nonlinear nano-plasmonics include nanolasers [7], nanoantenna [8], SPP based waveguides [9], nanostructure based optical limiters [10], nanoscopy [11, 12], nano-electronics as all optical ICs or transistors for information processing and storages [13], etc. For the evaluation of plasmonic nonlinear nano-photonics, one highly desirable tool is a technique that is capable to characterize nonlinearity from a single plasmonic nanostructure. Currently, various characterization techniques allow measurements of nonlinear optical constants such as absorption ($\boldsymbol{\beta}$) or refractive index ($\mathbf{n_2}$). These techniques include Z-scan (both $\boldsymbol{\beta}$, $\mathbf{n_2}$) [14], degenerate four-wave mixing (only $\mathbf{n_2}$) [15], nearly degenerate three-wave mixing (only $\mathbf{n_2}$) [16], optical Kerr gate and ellipse rotation (both $\boldsymbol{\beta}$, $\mathbf{n_2}$) [17], self-phase modulation (only $\mathbf{n_2}$) [18], Mach-Zehnder interferometry (both $\boldsymbol{\beta}$, $\mathbf{n_2}$) [19] etc. However, please note that all these methods measure nonlinearity in the bulk or thin films [20]. Among them, z-scan is probably the most widely adopted technique, due to its setup simplicity and capability to determine nonlinear refractive index and nonlinear absorption [21]. Below we briefly address the principle of z-scan and its limitations.

Z-scan technique is based on the measurement of transmittance as a “thin”sample moves along the propagation path (z-axis) of a focussed beam. The thickness of the sample should be smaller than the confocal parameter of the focus. In Z-scan, two measurement methods are used, namely, open-aperture and close-aperture. In the open-aperture setup, the transmitted light is completely collected by a large power detector. If there is no nonlinearity, the transmittance should be constant no matter

where the sample is. However, when nonlinear absorption exists, the transmittance changes as the sample is in the vicinity of the focus, where the intensity is highest along the beam path. Therefore, open aperture setup is sensitive to nonlinear absorption property, i.e. the imaginary part of the nonlinear refractive index. In the close-aperture setup, the transmittance is measured through a small aperture in front of the power detector, so the detected signal is sensitive to beam divergence/convergence, which is determined by the existence of nonlinear index (real part) in the thin sample. When there is no nonlinear index, the transmittance is again constant no matter where the thin sample is. With nonlinear refractive index, the sample acts like a z-dependent lens that modifies the transmission beam shape. In the close-aperture method, the power dependency in z direction quantifies the real part of nonlinear refractive index [21].

In brief, with linear responses, no change is expected during z-scan. Only when nonlinear response exists in the sample, the z-scan result deviates from a horizontal line, thus providing a high-sensitivity detection for nonlinearity. However, typically z-scan acquires nonlinear response from a thin sample, where multiple nanostructures are illuminated simultaneously, and collective behaviours are obtained. There have been extensive investigations by z-scan to study nonlinear absorption of thin plasmonic films [20], but not of single plasmonic nanostructure.

In this study, we propose a different method termed as “X-scan”, to characterise optical nonlinearity of a single nanostructure. The method is based on laser scanning microscopy, where an excitation focus moves in the lateral X-direction across a single nanostructure (thus the name X-scan). Similar to the requirement of z-scan, but converted into x direction, the diameter of the nanostructure should be much

smaller than the point spread function (PSF). At low excitation intensity, when there is no nonlinear response, due to convolution of laser PSF and the small nanostructure, a Gaussian profile is expected in the scanned image. Nevertheless, when nonlinearity exists in the nanostructure at high excitation intensity, the image profile is expected to deviate from Gaussian, thus providing high-sensitivity detection for nonlinearity, similar to z-scan.

In order to provide full characterization of the nanostructure nonlinearity, our X-scan technique is equipped with two optical detection paths, i.e. forward and backward detection paths, where the former determines the attenuation signal and the latter measures the backscattering signal. Similar to open- and close-aperture z-scan, our X-scan technique provides simultaneous absorption and scattering quantifications that are linked to imaginary and real parts of refractive index. Applying the novel two-path X-scan method to a single gold nanostructure, we have unravelled unprecedentedly large nonlinearities in both scattering and absorption, as we will show below.

Results and Discussion

Single plasmonic nanostructure measurement under microscope:

The schematic for the measurement of nonlinear absorption and scattering of a single plasmonic nanostructure under a standard laser scanning microscope is shown in figure 1(a). An inverted microscope is adopted, thus an excitation laser beam in upward direction is focussed on a single plasmonic nanostructure using an objective with numerical aperture (NA) equal to 1.4. The backscattered light is collected by the same high-NA objective, and the transmitted light is collected by a

condenser with NA 0.9. The large NAs in both paths ensure efficient collection of dipole scattering, which is the dominant scattering mode of a small nanostructure [22], in the microscope system. The laser excitation beam is raster scanned in lateral X- and Y-directions using a pair of galvanometer mirrors, allowing observation of PSF in both the forward and backward detection paths [23].

Figure 1(b) is a representative profile of “linear” backscattering from a single plasmonic nanostructure at low excitation intensity, and the inset gives the laser-scanning PSF. A Gaussian peak is typically observed, and the peak height quantifies the intensity of backscattering signal (R). Note that a confocal aperture in the backward detection path provides optical sectioning capability, and the nanostructure is typically immersed in oil to remove strong reflection from glass slides (see Methods).

On the other hand, a representative “linear” transmission profile due to a single plasmonic nanostructure is shown in figure 1(c). The laser-scanning PSF is given as an inset in figure 1(c), with a bright background and a dark spot in the center where nanostructure locates. The transmitted background represents the intensity of total excitation (T_o), which is equal to the sum of nanostructure-induced attenuation (A_{NP}) and transmission (T_{NP}). The dark spot in the image, i.e. the Gaussian dip in the signal profile of X-scan, quantifies the magnitude of attenuation.

From the backscattering and attenuation profiles, the absorption from a single plasmonic nanostructure is now ready to be quantified, as we explain in the following. It is well known that attenuation is composed of absorption and scattering. In our case, since transmission (T_{NP}) is collected in the forward path, attenuation (A_{NP})

becomes the sum of absorption and backscattering (R). As mentioned above, attenuation and backscattering are quantified in the forward and backward paths, respectively. By checking the linearity of the excitation and the detection system, and by calibrating signal intensities with glass reflection in the backward and forward paths (see Methods), absorption can be obtained by subtracting backscattering from attenuation, i.e. (A_{NP} – R). In the following, we present how the attenuation and backscattering of a single spherical gold nanostructure evolve from linear Gaussian to nonlinear profiles with increasing excitation intensity.

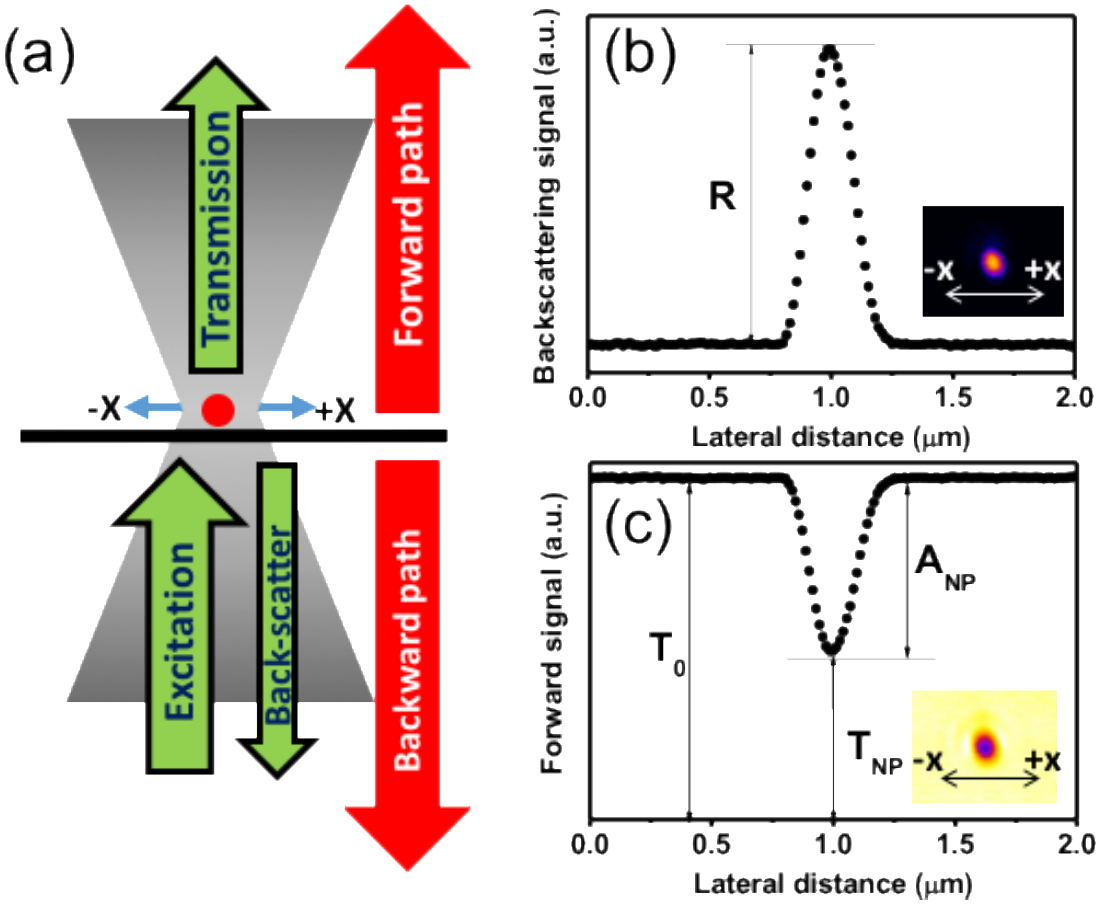

Figure 1:(a) *Schematic of X-scan method, i.e. excitation focus scanning in X direction. The back-scattering and transmission from a single nanostructure are separately recorded in backward path and forward path. (b) and (c) are representative profiles corresponding to the two detection. The peak value in*

(b) gives backscattering intensity R*, and the dip value of the transmission profile in (c) gives attenuation* A_{NP}*, from the same single plasmonic nanostructure.* T_0 *and* T_{NP} *denote laser intensity with direct transmission (no interaction with nanostructures), and transmission after the gold nanostructure, respectively.*

Linear response: Gaussian PSF

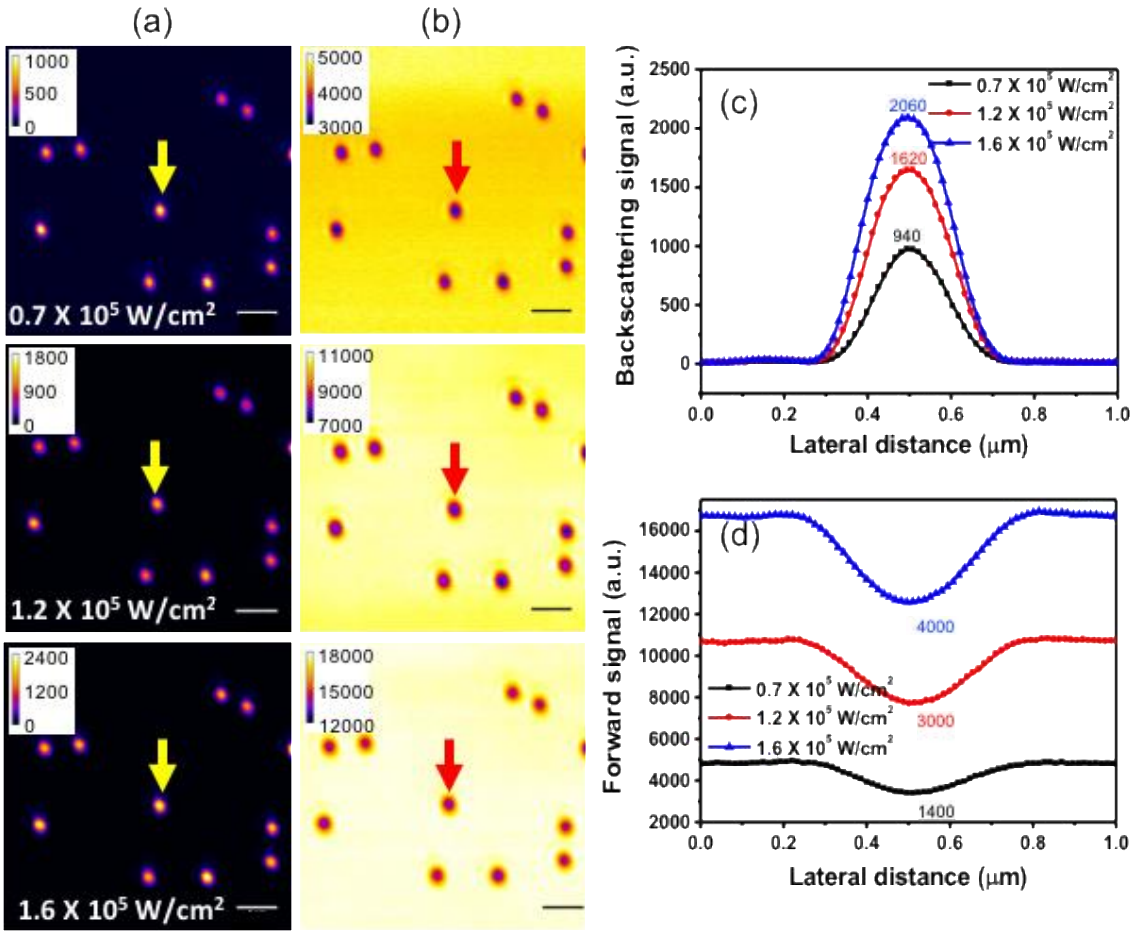

Figure 2: *(a) backward and (b) forward images of spherical gold nanostructures, at linear excitation regime. The "x-scan" signal profiles of the arrowed spherical gold nanostructures are given in (c) and (d), showing*

respectively linear increase of backscattering and attenuation versus excitation intensity. The number on each peak represents the signal quantity at centre of PSF (positive for backscattering and negative for attenuation). Scale-bar is 1μm.

As an application example, spherical gold nanostructures dispersed on glass surfaces are inspected with the two-channel X-scan method. Figure 2 gives the power-dependent scattering images and corresponding signal profiles in the low-power region, manifesting linear responses. Figures 2(a) and 2(b) are images acquired by the backward and forward beam paths respectively. Corresponding excitation intensities are given in each panel. Each image contains 10 particles, which exhibit similar signal intensities, indicating that not only the particles are uniform in size, but also the illumination intensity is even across the imaging region.

Figure 2(c) and 2(d) show the respective backscattering and attenuation profiles of a randomly selected single gold nanostructure, marked by an arrow in the image. Both the backscattering and attenuation profiles show nice Gaussian profiles, suggesting the optical responses are linear at low excitation intensity, as expected. The peak value and dip value (relative to the background) for each curve are given in the figures, showing that the backscattering and attenuation signal intensities indeed increase in proportion with the excitation intensity, further supporting the linear behaviour in this excitation intensity range.

Nonlinear response I: saturation of PSF

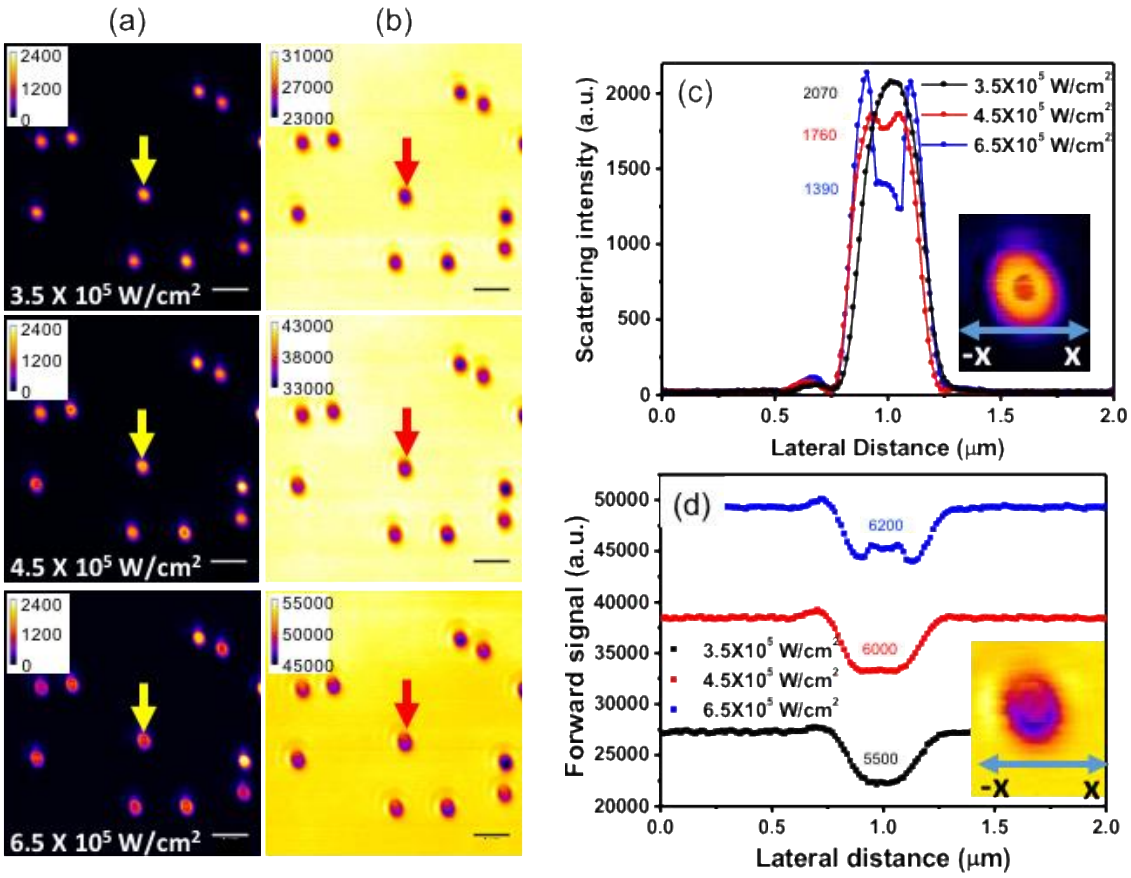

Figure 3:*(a) backward and (b) forward images of the same 10 spherical gold nanostructures as in Fig. 2, but with larger excitation intensity. The "x-scan" signal profiles of the arrowed spherical gold nanostructures are given in (c) and (d), showing respectively nonlinear responses of backscattering and attenuation versus excitation intensity. The number on each peak represents the signal quantity at centre of PSF (positive for backscattering and negative for attenuation). Scale-bar is 1μm*

When we increase the excitation intensity, interesting changes in the shape of PSF of a single spherical gold nanostructure are observed. Figures 3(a) and 3(b) show backward and forward images with increasing excitation intensity. Figure 3(c) and 3(d) give corresponding scattering and attenuation profiles, respectively. The zoom-in

images of one randomly selected spherical nanostructure are placed as insets of Figures 3(c) and 3(d). There are several interesting observations.

First, both forward and backward PSF profiles are no longer Gaussian, indicating the existence of nonlinearities in the X-scan technique. At excitation intensity of 4.5 x 10^5 W/cm^2, i.e. red curves in Fig. 3(c) and 3(d), nearly flattop PSFs are observed in both channels, manifesting the “saturation” behaviour of both scattering and attenuation.

Second, as excitation intensity increase to 6.5 x 10^5 W/cm^2, i.e. blue curves in Fig. 3(c) and 3(d), splitting of one peak (or dip) into two lobes were observed in both channels, leading to doughnut-like shapes shown in the insets. Since the excitation has a Gaussian profile, whose intensity is highest in the centre of PSF, the doughnut-like responses thus indicate that the amplitude of scattering and attenuation decrease with increasing excitation intensity. This is a very non-intuitive result, but the doughnut PSF can be observed in all particles of Fig. 3(a) and 3(b). We will discuss the mechanism of this unexpected nonlinear response in a later section.

Third, from the quantitative number on each peak in Fig. 3(c) and 3(d), backscattering drops quickly while attenuation increases slowly. As mentioned earlier, attenuation is composed of absorption and scattering, and with a proper calibration, we are able to quantify absorption through the two-channel measurement. Therefore, the difference in scattering and attenuation responses predicts the absorption nonlinearity would be different from scattering nonlinearity.

Nonlinear response II: reverse saturation of PSF

By further increasing the excitation intensity, i.e. above 10^6 W/cm^2, more interesting changes in the PSFs of individual gold nanostructure is observed in both detection paths. Again, figures 4(a) and 4(b) are images, and figures 4(c) and 4(d) are corresponding PSF profiles. Different from the saturation behaviour in the previous section, now at ~10^6 W/cm^2 excitation intensity, a new peak emerges at the center of the PSFs, manifesting the “reverse saturation” behaviour. Although the phenomenon is more clearly visible in the scattering curves of Fig. 4(c) than in attenuation of 4(d), from quantitative value on each curve, both scattering and attenuation increase at this reverse saturation regime.

As excitation intensity increase to 1.5 x 10^6 W/cm^2, the shape of the new peak becomes evident, especially in the backward channel of Figure 4(c). Apparently, the new peak has a much smaller FWHM compared to the original diffraction-limited PSF, e.g. those in Fig. 2. The small FWHM of the reverse saturation peak implies that the amplitude of scattering and attenuation increase faster than increasing excitation intensity, i.e. the power dependency in this region (slope of output versus input) exceeds that of the linear region. By decomposing attenuation into scattering and absorption, we are going to present the power dependencies of these optical interactions in the next section.

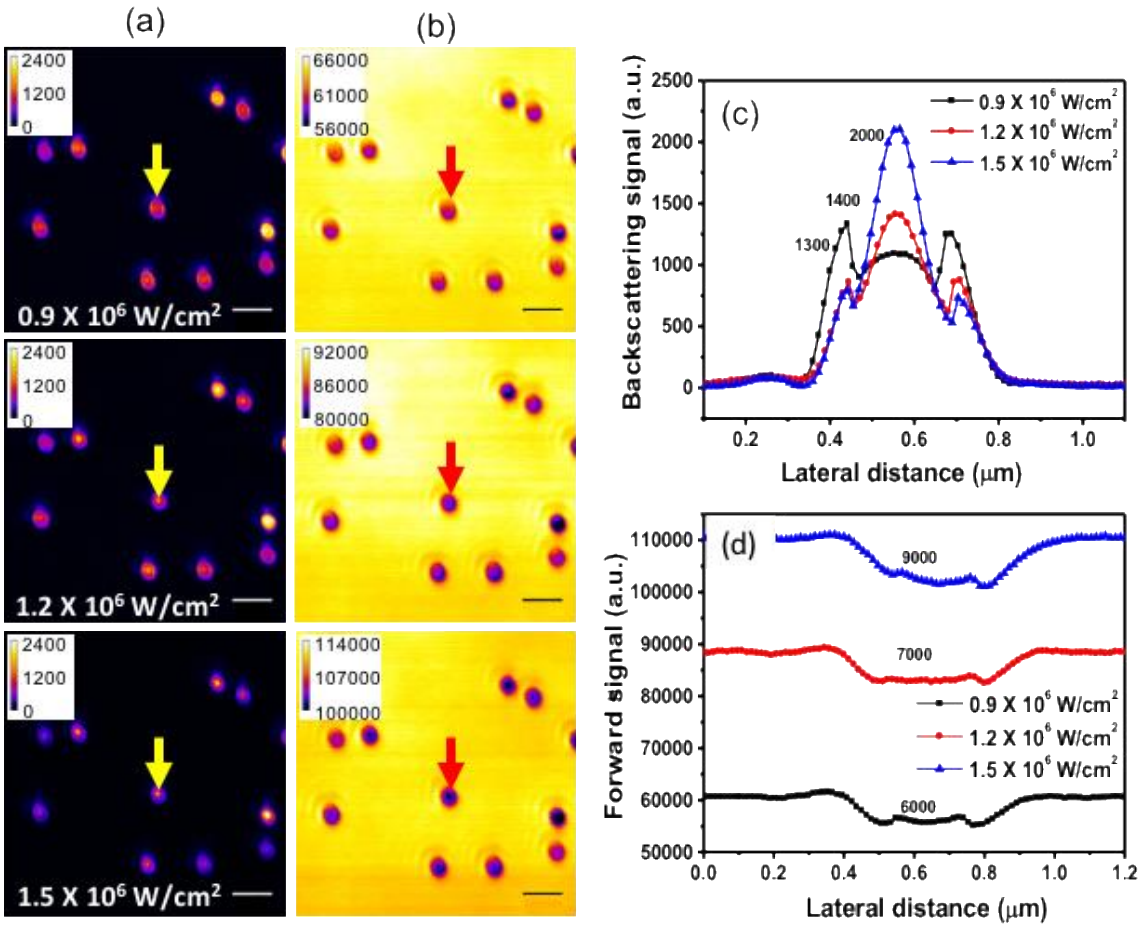

Figure 4: *(a) backward and (b) forward images of the same 10 spherical gold nanostructures as in Fig. 3, but with further larger excitation intensity. The "x-scan" signal profiles of the arrowed spherical gold nanostructures are given in (c) and (d), showing respectively nonlinear responses of backscattering and attenuation versus excitation intensity. The number on each peak represents the signal quantity at centre of PSF (positive for backscattering and negative for attenuation, considering the change in PMT voltages during measurements). Scale-bar is 1μm.*

Summarizing nonlinear behaviors:

In figures 2 – 4, backward and forward signals from ten plasmonic gold nanostructures are recorded at increasing excitation intensity. From these image profiles, the intensity-dependent attenuation and scattering are plotted in Fig. 5(a) (blue and red dots). As described in figure 1, absorption can be derived from (A_{NP} – R) (green dots in Fig. 5(a)). It is very interesting to see that absorption has a different dependency from scattering. The latter shows dramatic saturation and reverse saturation behavior, while the former has mainly the saturation one.

To better understand it, we plot the percentage of each different signal (attenuation, transmission, backward scattering, absorption) in figure 5(b). The definition of each signal has been described in figure 1 (attenuation A_{NP}, transmission T_{NP}, backward scattering R), and absorption is (A_{NP} – R). As mentioned in figure 1, the total excitation intensity is derived from T_0 of forward images. Since it increases proportionally to the incident intensity, we normalized "Total" in figure 5 to be unity (black dots), and all other signals were accordingly normalized. These normalized values can be viewed as the efficiency of gold nanostructure interacting with light, and should be proportional to corresponding cross sections. Apparently, T_{NP} (purple dots) + A_{NP} (blue dots) = T_0, which holds true no matter in linear or nonlinear regime, as also shown in figure 5(b).

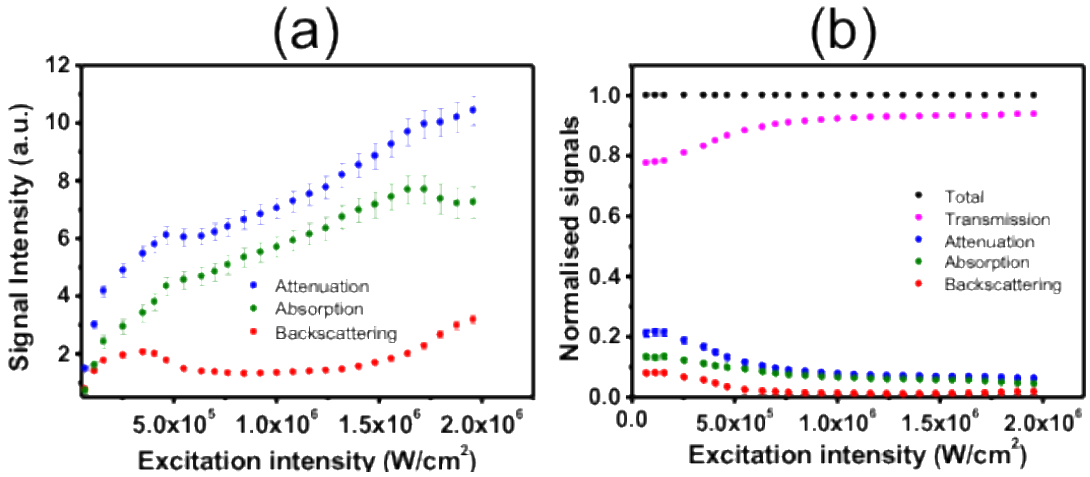

Figure 5: *(a) Excitation intensity dependency of attenuation (blue), absorption (green), and backscattering (red) signals. (b) Normalized signals (i.e. proportional to corresponding cross-sections) versus excitation laser intensity.*

In the linear regime, we find that backward scattering efficiency is constant at ~8% (red dots), which is about half of absorption (14%, green dots). This ratio is consistent with Mie theory calculation, confirming the correctness of our signal calibration. According to Mie theory, forward scattering should be equal to backward scattering for this nanostructure. In our measurement, the transmission T_{NP} is 79% in this linear region, containing both forward scattering and photons that not interact with nanostructures. Therefore, the true forward scattering contribution should be only 8%, and 71% is due to the non-interacted transmission.

In the nonlinear region, i.e. excitation intensity above 2 x 10^5 W/cm^2, both attenuation and backscattering efficiencies drop, but interestingly with different slopes. Apparently the particle becomes more transparent at high excitation intensity (attenuation reduce significantly). Corresponding absorption efficiency at each intensity is found by (A_{NP} – R), and also exhibits reduction, i.e. saturation of absorption is observed.

It is remarkable to see that the trend of attenuation and absorption nonlinearities are quite different from that of backscattering nonlinearity. In the saturation region (between 0.2– 0.8 MW/cm^2), the strengths of both absorption and backscattering drop by 7% (absorption 13.5% → 6.5%; backscattering 8% → 1%). However, the

former changes only two folds, while the latter is eight fold, i.e, the backscattering decay is in cubic order larger than absorption.

One possible reason could be that scattering is related to square of dielectric constant variation, while absorption is linearly proportional to dielectric constant. That is, with dipolar oscillation of free electrons in conduction band, the absorption and scattering cross-sections from a plasmonic nanosphere can be determined by classical Mie theory as:

$$C_{abs} = 4\pi k r^3 Im\left(\frac{\varepsilon_p - \varepsilon_m}{\varepsilon_p + 2\varepsilon_m}\right)$$

$$C_{sca} = 8\pi k^4 r^6 \left|\frac{\varepsilon_p - \varepsilon_m}{\varepsilon_p + 2\varepsilon_m}\right|^2$$

where, k is the wave vector, r is the radius of particle, ε_p is the dielectric constant of the particle, and ε_m is the dielectric constant of the surrounding medium. With high intensity laser illumination, photothermal effect induces particle permittivity change, leading to the nonlinear effect. However, this equation only accounts for a square order difference.

The above equation considers total scattering cross-section. Nevertheless, in our experiment, only backscattering is quantified. Therefore, another possible factor is asymmetric scattering due to interference between high-order poles, i.e. backscattering strength is no longer similar to forward scattering. Recently there were many reports [25-27] on directional scattering via multi-pole interferences in plasmonic nanostructures. However, most of them rely on specially designed structures to couple magnetic dipole and electric dipole. More studies are necessary

to quantify forward scattering at the same time to verify this possibility of directional scattering at heated plasmonic nanostructure.

Another difference between backscattering and absorption in figure 5 is that only the former exhibits clear reverse saturation effect. It might be due to additional thermal effect of the surrounding medium (immersion oil). Once again, further studies will be necessary to quantify the temperatures of nanostructure, as well as of immersion medium, to provide a better explanation of the complicated photothermal nonlinearity.

Conclusion

In this report, we successfully demonstrate simultaneous measurement of the nonlinear attenuation, absorption and scattering in a single plasmonic nanostructure using the two-path X-scan method for the first time. Unlike Z-scan, this X-scan method, which is based on a laser scanning microscope, is capable to characterize/visualize nonlinear response from the PSF of a single nanostructure. With the simultaneous forward and backward measurement, we have quantified nonlinearities in absorption and scattering, which show surprisingly different behaviors that may lead to optical cloaking and directional emission of a single heated nanostructure.

Methods

The experimental setup is shown in figure 6(a), which was based on a modified confocal laser scanning microscope (IX71+FV300, Olympus, Japan). A CW laser beam of wavelength 561 nm (Jive™ 561 nm, Cobolt, Sweden) was sent through a pair of built-in galvo-mirrors, and then focused on plasmonic nanostructures by an

objective UPlanSApo 100x/NA1.4, Olympus, Japan), to form two-dimensional raster scan at its focal plane. The power of laser excitation was fine-tuned through neutral density (ND) filters. The back-scattered signals from the plasmonic nanostructures were collected through the same objective, separated from the incident beam with a 50/50 beam splitter, spatially filtered by a confocal aperture, to reach backward photomultiplier tube (PMT) detector. On the other hand, transmission signal passed through the plasmonic sample and was collected by a condenser (U-LTD/NA 0.9, Olympus, Japan) to reach the forward PMT detector directly without confocal aperture. Both forward and backward images were formed on a computer by synchronizing the PMT signal and the scanner. Due to the different collection paths and PMT sensitivities in forward and backward paths, it is important to calibrate their signal with each other to determine absorption signal, as shown below.

Fig. 6(b) is the forward (transmission) and backward (reflection) signals from a cover glass when gradually increasing excitation intensity. In this case, the backward signals came from air-glass interface reflection at the top of cover glass, and the rest excitation photons transmitted to form the forward signals. The perfect linear dependencies of both signals verified that no nonlinearity is induced in the optical excitation and detection system. In addition, the air-glass reflection should be 4%, and 96% of the excitation photons were transmitted. so the forward and backward signal were calibrated accordingly, as shown in Fig. 6(c). The same calibration was applied to figures 2-5 in the main text.

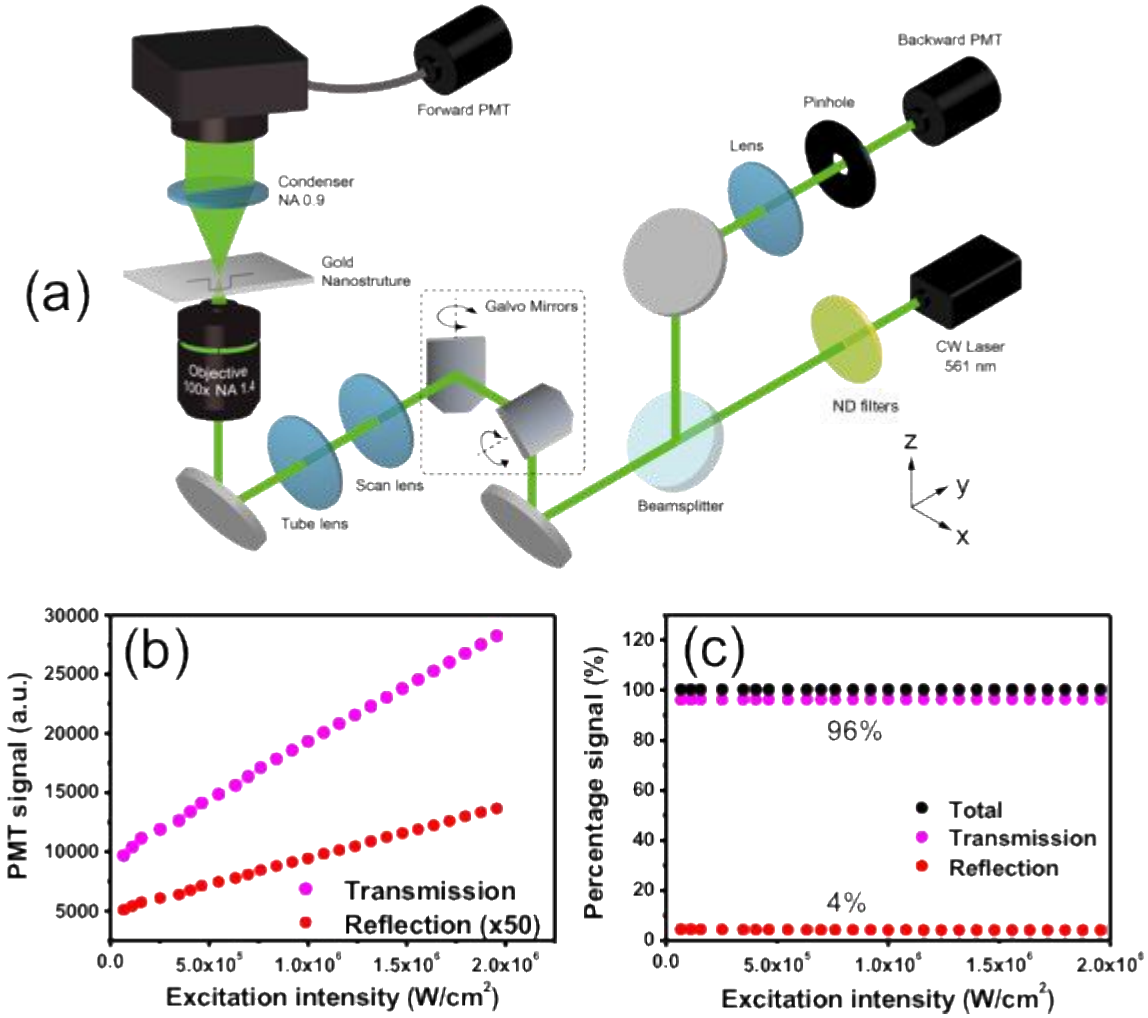

Figure 6: *(a) Schematic of experimental set-up of laser scanning system on an inverted microscope. (b) Linearity test of backward and forward signals from the partial reflection and transmission of a cover glass. It is obvious that no nonlinearity is induced in the microscope system. (c) The forward and backward signals are calibrated to correctly represent 4% reflection and 96% transmission from an air-glass interface. The same calibration applies to all signal processing in the main text.*

Sample preparation

The sample was 80 nm diameter gold nanospheres commercially available from BBI Solutions, UK. Before use, the nanostructure solution was sonicated for 2 minutes to avoid particle aggregation. Then one drop of the solution was placed on polysine slides (Thermo Fisher Scientifics, MA) for 20 seconds, gently rinsed with deionised water, and dried with nitrogen purge. The sample was immersed in index-matching oil to remove glass reflection.

Acknowledgements

This study was supported by the Ministry of Science and Technology of Taiwan, under grant MOST-108-2321-B-002-058-MY2 and MOST-105-2628-M-002-010-MY4. Tushar Jagadale and Dhanya Murali were funded through MOST-106-2811-M-002-198 and MOST-107-2811-M-002-3067, respectively. Tushar Jagadale also acknowledges DST-GOI for the support under IFA-13-PH-73. Shi-Wei Chu acknowledges the generous support from the Foundation for the Advancement of Outstanding Scholarship.

References

1. Deka, G; Sun, C.K.; Fujita, K; Chu, S.W. *Nanophotonics*, 2017, *6*, 31-49.
2. Kauranen, M; Zayats, A.V. *Nature Photonics,* **2012,** *6,* 737-748.
3. Schuller, J.A.; Barnard, E.S.; Cai, W; Jun, V.C.; White, J.S.; Brongersma, M.I. *Nature Materials,* **2010,** 9, 193-204.
4. Willets, K.A.; Wilson, A.J.; Sunderesan, V.; Joshi, P.B. *Chem. Rev.,* **2017,** *117,* 7538-7582.
5. Stockman, M.I. *Optics Express,* **2011,***19*, 22029-22106

6. S. B. Ogale, A. Ahmad, R. Pasricha, V.V. Dhas and A. Syad *Appl. Phys. Lett*., **2006,** 89, 263105-263107
7. Oulton, R.F.; Sorger, V.J; Zentgraf, T; Ma, R-M; Gladden, C; Dai, L; Bartal, G; Zhnag, X *Nature*, **2009**, 461, 629-632.
8. Kinkhabwala, A.; Yu, Z.; Fan, S.; Avlasevich, Y; Mullen, K; Moerner, W.E. *Nature Photonics,* **2009,** *3,* 654-657.
9. Fang, Y; Sun, M *Light: Science & Applications,* **2015,** *4,* e294-11.
10. Sun, Y.P.; Riggs, J.E.; Henbest, K.B.; Martin, R.B. *Journal of Nonlinear Optical Physics & Materials,* **2000,** *9,* 481-503.
11. Chu, S.W.; Su, T.Y.; Oketani, R.; Huang, Y.T.; Wu, H.Y.; Yonemaru, Y.; Yamanaka, M.; Lee, H.; Zhuo, G.Y.; Lee, M.Y.; Kawata, S.; Fujita, K. *Phys Rev Lett,* **2014,** *112,* 017402-04.
12. Wu, H.Y.; Huang, Y.T.; Shen, P.T.; Lee, H.; Oketani, R.; Yonemaru, Y.; Yamanaka, M.; Shoji, S.; Lin, K.H.; Chang, C.W.; Kawata, S.; Fujita, K.; Chu, S.W. *Sci. Reports*, **2016,** *6,* 24293-9.
13. Fang, X,; MacDonald, K.F.; Zheludev, N.I. *Light: Science & Applications,* **2015,** *4,* e292-7.
14. Kostritskii, S.M.;Aillerie, M.;Kokonyan, E.; Sevostyanov, O.G*. J. Phys.: Conf. Ser.,* **2017,***879,* 012003
15. Munk, D; Katzman, M.; Westreich, O.; Nun, M.B.; Lior, Y.; Sicron, N.; Paltiel, Y.; Zadok, A. *Optical Materials Express*, **2018**, *8*, 66-72.
16. Slabko, V.V.; Popov, A.K.; Tkachenko, V.A.; Myslivets, S.A. *Optics Letters*, **2016**, *41*, 3976-3979.
17. Sun, Q.; Liu, H.; Huang, N.; Wang, Z.; Li, S.; Han, J *Laser Physics*, **2015**, 25, 125403-4.

18. Liu, X.; Driscoll, J.B.; Dadap, J.I.; Osgood Jr., R.M.; Assefa, S.; Vlasov, A.Y.; Green W.M.J. *Optics Express*, **2011,** *19***,** 7778-7789.
19. Srivastva, A.; Medhekar, S *Optics & Laser Technology*, **2011**, 43, 1208-1211.
20. Zakery, A; Elliot S.R. *Springer series in optical sciences*, **2007,**ISBN-13 978-3-540-71066-0, 1-207.
21. Sheik-Bahae, M; Said, A.A.; Van Stryland, E.W. *Opt. Lett.,* **1989,** *14,* 955-957.
22. Bohren, C.F.; Huffman, D.R. *Wiley VCH,* **1998,** *ISBN978-O-471-29340-8.*
23. Chen, Y.T.; Lee, P.H.; Shen, P.T.; Launer, J.; Oketani, R.; Li, K.Y.; Huang, Y.T.; Masui, K.; Shoji, S.; Fujita, K.; Chu, S.W. *ACS Photonics,* **2016,***3,* 1432−1439.
24. Chu, S.W.; Wu, H.Y.; Huang, Y.T.; Su, T.Y.; Lee, H.; Yonemaru, Y.; Yamanaka, M.; Oketani, R.; Kawata, S.; Shoji, S.; Fujita, K.*ACS Photonics,***2014,***1,* 32–37
25. Mirin, N.A.; Halas N.J. Nano Letters, **2009**, 9, 1255-1259
26. Shegai T.; Chen S.; Miljković V.D.; Zengin G.; Johansson P.; Käll M. Nature Communications, **2011**, 2, 481
27. Liu W.; Miroshnichenko A. E.; Neshev D. N.; Kivshar Y. S. ACS Nano, **2012**, 6, 5489-5497